CRYSTAL GROWTH & DESIGN

Article

Investigating a soluble pharmaceutical salt: Albendazole Hydrochloride

Agustina Bongioanni, Maria Soledad Bueno, Julieta Abraham Miranda, Ana Karina Chattah, Alejandro Pedro Ayala, Marcela Raquel Longhi, and Claudia Garnero

Cryst. Growth Des., **Just Accepted Manuscript** • DOI: 10.1021/acs.cgd.9b00348 • Publication Date (Web): 19 Jun 2019

is published by the American Chemical Society. 1155 Sixteenth Street N.W., Washington, DC 20036

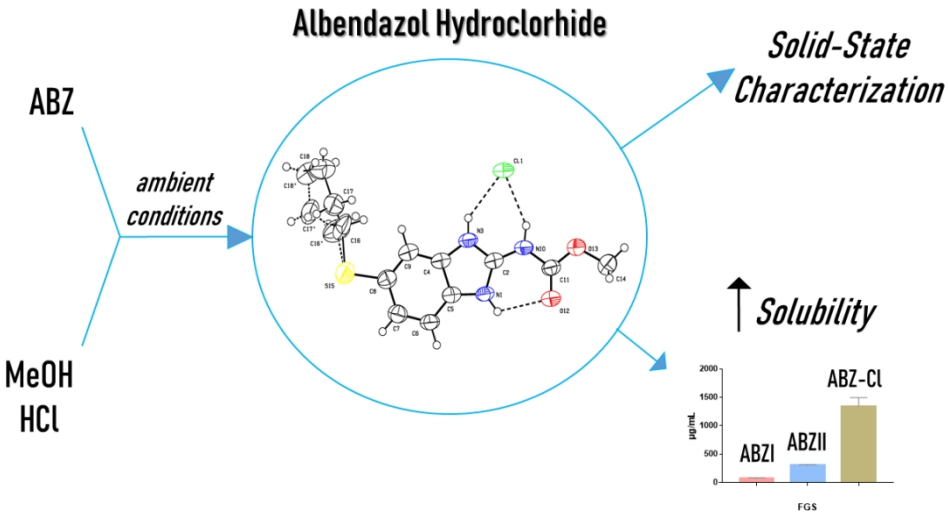

338x190mm (96 x 96 DPI)

Investigating a soluble pharmaceutical salt: Albendazole Hydrochloride

Agustina Bongioanni[1]; Maria Soledad Bueno[1]; Julieta Abraham Miranda[1]; Ana Karina Chattah[2]; Alejandro Pedro Ayala[3]; Marcela Raquel Longhi[1]; Claudia Garnero[1]

[1]Departamento de Ciencias Farmacéuticas, Facultad de Ciencias Químicas, Universidad Nacional de Córdoba, and Unidad de Investigación y Desarrollo en Tecnología Farmacéutica (UNITEFA) CONICET-UNC, Ciudad Universitaria, X5000HUA, Córdoba, Argentina.

[2]Facultad de Matemática, Astronomía, Física y Computación, Universidad Nacional de Córdoba and IFEG (CONICET), Ciudad Universitaria, X5000HUA, Córdoba, Argentina.

[3]Departamento de Física, Universidade Federal do Ceará, Fortaleza, Ceara, Brazil.

ABSTRACT

Albendazole is an effective antihelmintic drug, which has an unpredictable therapeutic response due to its low solubility in biological fluids that limits its oral absorption. In an attempt to improve solubility, Albendazole Hydrochloride, a soluble pharmaceutical salt, was obtained and characterized by X-ray diffraction together with magic angle spinning solid-state nuclear magnetic resonance spectroscopy, Raman and Fourier transform infrared spectroscopies, thermal analysis, energy-dispersive X-ray spectroscopy and scanning electron microscopy. These studies revealed that the crystalline habit of Albendazole Hydrochloride is different from that of the Albendazole solid forms previously reported. Full structure was elucidated by performing single-crystal X-ray diffraction. The characterization studies showed the participation of the carbamate moiety in the salt formation. In addition, the solubility studies showed a significant increase in solubility with respect to forms I and II of Albendazole. In conclusion, our results point to that Albendazole Hydrochloride can be an auspicious salt to be used as a new product in an attempt to counteract unfavorable pharmaceutical properties.

KEYWORDS: Albendazole Hydrochloride, characterization, X-ray diffraction, solid-state nuclear magnetic resonance, solubility

1. INTRODUCTION

The soil-transmitted helminthiasis is a constant concern within public health, affecting the vulnerable socioeconomic sectors with high impact. These parasitic infections are endemic and widely distributed in tropical and subtropical areas, affecting more than 1.5 billion people worldwide. These helminthiasis cause alterations in the nutritional, cognitive and physical development of the population, so their treatment should be essential and priority.[1-4]

Benzimidazole derivatives are the most used compounds with acceptable antihelminthic efficacy. Albendazole (ABZ), one of the drugs of choice, displays a broad spectrum of antihelminthic action, interfering with microtubule assembly and blocking glucose uptake in many intestinal and tissue nematodes and some cestodes.[5-7] It is widely used by oral administration; however, its efficacy is often limited by its poor absorption in the gastrointestinal tract, due to its poor aqueous solubility and its slow rate of dissolution. Therefore, treatments with high doses are required, which often have undesirable side effects associated.[8,9] Two solid forms, designated ABZI and ABZII, which have been previously reported by our group, showed significant differences in their chemical and physical properties including solubility.[10,11]

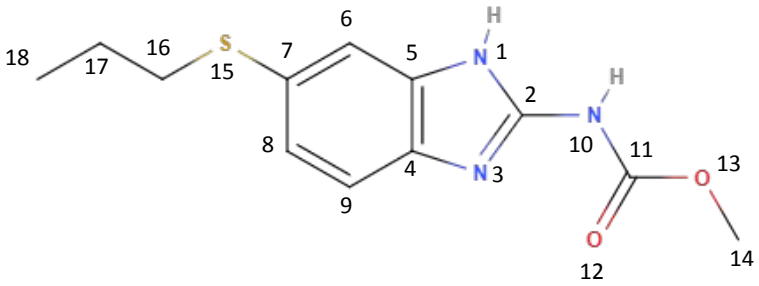

Scheme 1. Chemical structure of ABZ along with the atom numbering adopted.

In order to counteract the negative properties of ABZ and optimize the chemotherapeutic treatment, the development of innovative systems for an adequate therapy is of relevant importance for the pharmaceutical sciences. Different strategies have been studied, such as complexation with cyclodextrins[11-14] or maltodextrins,[15] solid dispersions,[16,17] and nanocrystals[18] among others. Another effective option is the incorporation of pharmaceutically acceptable coformer agents that do not alter the covalent bond of the drug.[19] In this context, the formation of soluble salts can be a promising solution. Particularly, the amine salts are more soluble than their precursor and less

susceptible to decomposition by oxidation and other reactions. For this reason, many active pharmaceutical ingredients are formulated and stored as their salts. In addition, the hydrochloride salts are the most used in the pharmaceutical industry.[20]

In the literature, Albendazole salts were obtained using a variety of possible counterions: hydrochloric acid, methane sulfonic acid, sulfuric acid and para-toluene sulfonic acid.[21,22] Also, salts and salt hydrates with sulfonic acids (benzene and *p*-toluene sulfonic acid) and carboxylic acids (oxalic acid, maleic acid, L-tartaric acid, 2,6-dihydroxybenzoic acid and 2,4,6-trihydroxybenzoic acid) were reported.[23] Based on their characterization studies some differences between them were evidence.

The aim of the present study was to obtain a soluble salt of ABZ that allows optimizing its biopharmaceutical properties. Albendazole Hydrochloride (ABZ-Cl), a stable and soluble salt, was synthesized, isolated and physicochemically characterized with various techniques, evaluating its effect on the solubility.

2. EXPERIMENTAL SECTION

Chemicals and Reagents

Albendazole (ABZ) was provided by Todo Droga (Argentina). Methanol and hydrochloric acid, analytical reagent grade chemicals, were obtained from Cicarelli (Argentina). A Millipore Milli Q Water Purification System (Millipore, Bedford, MA, USA) generated the water used in these studies. All other chemicals were of analytical grade.

Obtaining Albendazole Hydrochloride

In an attempt to produce ABZ-Cl, ABZ form I (approximately 10 mg) was dissolved in 10 mL of a solution of hydrochloric acid (0.084 M) in methanol at room temperature, and then allowed to a slow complete evaporation of the solvent. Pink crystals were collected after 5-6 days.

X-ray Diffraction measurements

The diffraction data from ABZ-Cl crystals were collected on a Bruker D8 VENTURE Kappa geometry diffractometer, equipped with a PHOTON II CPAD detector, a MoKα INCOATEC IμS 3.0 microfocus source (λ = 0.71073 Å) and APEX 3 control software.[24] Data reduction was performed using SAINT[24]

and the intensities were corrected for absorption using SADABS.[25] Using Olex2,[26] the structure was solved by intrinsic phasing using SHELXT[27] and refined by full-matrix least squares using SHELXL.[28, 29] All non-hydrogen atoms were refined anisotropically. Hydrogen atom positions were calculated geometrically and refined using the riding model. The crystallographic information file of ABZ-Cl crystal was deposited in the Cambridge Structural Data Base,[30,31] under code CCDC 1879541. Copies of the data can be obtained, free of charge, via www.ccdc.cam.ac.uk.

Powder X-ray diffraction (PXRD) patterns were obtained at ambient temperature using a Philips PW1710 diffractometer operating at 45 kV and 30 mA with Cu-Kα radiation. The powder pattern was collected by scanning 2θ from 2° to 40° with a step size of 0.05° at a scanning rate of 2.5 seconds/step, at the initial time and after six months of storage.

Solid-State NMR Spectroscopy (ssNMR)

All ssNMR experiments were performed at room temperature in a Bruker Avance II spectrometer, operating at 300.13 MHz for protons, equipped with a 4 mm MAS probe. Ramp cross polarization/magic angle spinning (CP-MAS) sequence with proton decoupling during acquisition was used to obtain high resolution solid state ^{13}C spectra of ABZ-Cl.[32,33] The compound was evaluated at two different times (initial time and after six months of storage). The operating frequency for carbons was 75.46 MHz, using Glycine as an external reference. Spectra were recorded with 1600 scans, setting a contact time of 1.5 ms and a recycling time of 5 s. SPINAL-64 was used for proton decoupling during acquisition.[34] The edition spectrum containing quaternary carbons and methyl groups was also recorded.[32] The spinning rate in these experiments was set to 10 kHz.

2D ^{1}H -^{13}C heteronuclear correlation (HETCOR) spectrum was recorded at 10 kHz MAS following the sequence presented by van Rossum et al.[35] The pulse sequence starts with a train of off-resonance frequency-switched Lee−Goldburg (FSLG) pulses in a tilted frame at the magic-angle, to cancel the first two terms of the homonuclear dipolar coupling Hamiltonian. FSLG irradiation was applied during the t1 evolution period in successive times τ. A ramped-amplitude CP sequence enhanced ^{13}C signals, and the SPINAL-64 decoupling was also used during ^{13}C acquisition. The period τ was set to 7.68 μs. The CP contact time was set to 200 μs to avoid homonuclear spin-diffusion, and the recycle delay was 5 s. Magic-angle pulse was set to 2.55 μs. Sixty-four t1

increments with a dwell time of 35.5 μs, corresponding to a total acquisition time of 1.14 ms, were used.

Raman spectroscopy

Raman spectra were recorded on a LabRAM HR (Horiba) spectrometer equipped with a liquid N2-cooled CCD detector using a near infrared laser (785nm) for excitation, with a power of 100 mW. The spectral region studied was 50-4000 cm^{-1} and the measurements were carried out using a 50x NIR microscope objective, with an acquisition time of 150 s by region.

Fourier-transform infrared spectroscopy (FT-IR)

The FT-IR spectra were recorded on a Nicolet 5 SXC FT-IR Spectrophotometer (Madison, WI, USA), with potassium bromide disks prepared by compression.

Thermal analysis

Simultaneous differential scanning calorimetry (DSC) and thermogravimetric analysis (TGA) experiments were performed on a Jupiter STA 449 F3 Jupiter (Netzsch) system. Measurements were obtained over a temperature range of 30-450 ºC using a heating rate of $10°C.min^{-1}$ and a sealed aluminum crucible with pierced lids containing 5 mg of sample. The sensors and the crucibles were under a constant flow of nitrogen (70 mL/min) during the experiment.

Scanning electron microscopy studies (SEM) - Energy-dispersive X-ray spectroscopy (EDS)

Microscopic morphological structure of the solid-state sample was investigated and photographed using a Carl Zeiss Sigma scanning electron microscope. The sample was fixed on a brass stub by means of a double-sided aluminum tape, which was gold-coated under vacuum using a sputter coater Quorum 150 to improve the conductivity. The EDS spectrum was acquired using an Oxford energy dispersive silicon drift detector, which has an X-ray detector attached to it, an 80-mm^2 front area and a 127 eV nominal resolution for Mn-Kα line. The chemical composition of the sample was identified using an external PC.

Solubility Studies

The apparent solubility of ABZ-Cl in aqueous solution, simulated gastric fluid (SGF) and simulated intestinal fluid (SIF) was studied. An excess of ABZ-Cl (approximately 20 mg) was placed in stoppered tubes containing 5 mL of each media. The suspensions were agitated in an ultrasonic bath (Elmasonic S40) and then maintained at 37.0 ± 0.1 ºC for 72 h in a constant-temperature water bath (Pilot One, Huber). After that, the remaining solid was removed by filtration through a 0.45 μm membrane filter (Millipore, USA). The clear solutions were suitably diluted and analyzed by UV-Vis spectrophotometry (Agilent Cary 60 spectrophotometer) at λ = 292 nm.

3. RESULTS AND DISCUSSION

Solid-State Characterization

In order to characterize and unequivocally distinguish the solid sample ABZ-Cl, several complementary techniques such as X-ray diffraction experiments, ssNMR, Raman and FT-IR spectroscopy, DSC, TGA, EDS and SEM were used. The results were compared with those obtained for the characterization of both ABZ solid forms (ABZ I and ABZ II) in our previous reports.[10,15]

Single-Crystal X-ray diffraction

Adequate fragments from single-crystal samples were selected and used as material for the experiments. We determined that ABZ-Cl crystallizes in a triclinic system with $P\bar{1}$ space group, and two molecules per unit cell and the following lattice parameters: a=7.5578(5) Å, b=7.7829(5) Å, c = 12.8313(9) Å, α = 78.980(2)º; β= 84.596(2)º and γ = 79.119(2)º (Table S1). Figure 1 shows the thermal ellipsoid representations of the molecular structure for ABZ-Cl, together with atomic numbering scheme. The asymmetric unit is characterized by the disorder of the propanethiol tail, as well as, a slight positional disorder of the chlorine ion. Since the compound crystallizes as a salt, all nitrogen atoms are protonated. The carbamate tail is aligned in the plane of the aromatic rings by the intramolecular hydrogen-bond N1H1···O12 (2.764(2) Å).

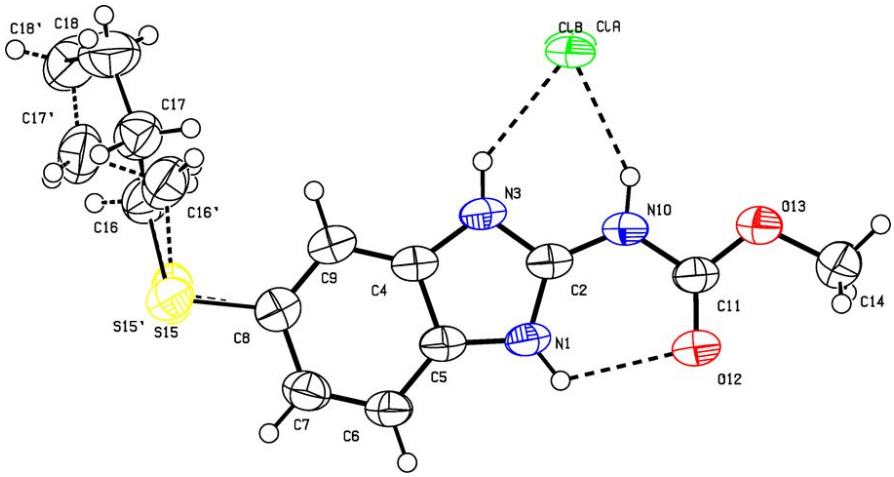

Figure 1. ORTEP plot of ABZ-Cl drawn at 50% probability level.

Figure 2a shows the unit cell of ABZ-Cl, where the two molecules in the unit are aligned antiparallel, with their aromatic rings lying approximately parallel to the (101) plane. The crystalline structure is stabilized by chains along the [010] direction, where ABZ and Cl are alternated and linked by hydrogen-bonds. On one side of the ABZ molecule, there is a bifurcated hydrogen bond N3H3···ClA/B (3.100(5)/3.023(16) (Å) and N10H10···ClA/B (3.129(5)/3.05(2) Å). The following ABZ molecule is linked to Cl by a single bond N1H1···ClA/B (3.154(5)/3.18(2) Å), as shown in Figure 2b. This packing differs from the one observed in ABZ polymorphs, whose main features are ABZ $R_2^2(8)$ dimers based on NH···N bonds.[36] A similar packing is observed in the polymorphs of mebendazole, another benzimidazole carbamate derivative.[37] In fact, those dimers are also disrupted by an halide cation in mebendazole hydrochloride and hydrobromide salts, which exhibit the same alternated chains as ABZ-Cl.[38, 39]

The alternated chains are stacked linked by π-π interactions, as it is clearly evidenced by the Hirshfeld surface mapped with the shape index[40] presented in Figure 3. The complementary red and blue triangles in a 'bow-tie' pattern on the surface are well-known markers of close C…C interplanar contacts characteristic of a π-π bond.[41] Thus, on one side of the ABZ molecule, the antiparallel chains are linked by a π-π bond connecting the six-membered rings (Figure 3a), whose centroids are separated by 3.7051(13) Å. On the other ABZ side, three 'bow-tie' patterns can be identified (Figure 3b). Two of them are related to the phenyl-imidazol π-π bond (3.5814 (11) Å), while the third is associated to the bond between imidazole rings (3.5482(11) Å). Similar π-π interactions can be

identified in the mebendazole hydrochloride and hydrobromide salts,[36,37] being a characteristic of the packing of the antiparallel chains in benzimidazole carbamate derivative inorganic salts.

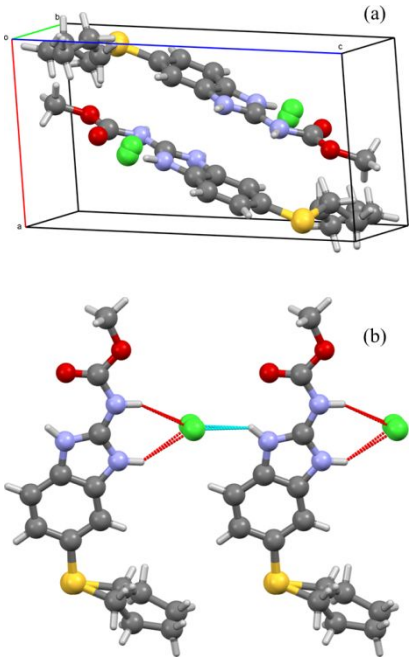

Figure 2. (a) Unit cell and (b) alternated chains along the b-axis of ABZ-Cl.

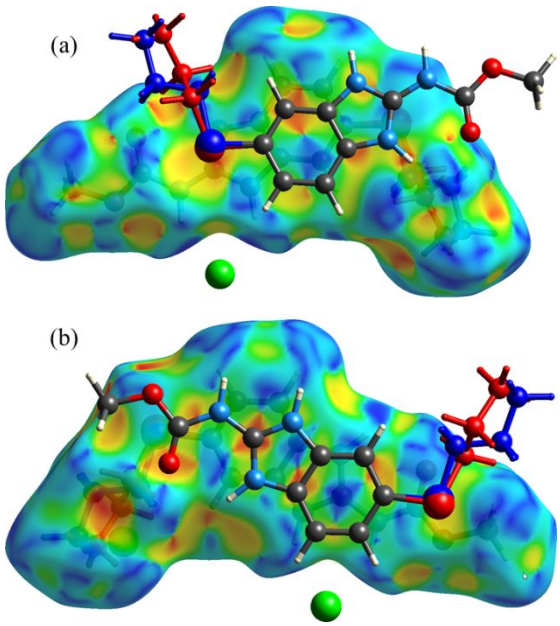

Figure 3. Shape index mapped Hirshfeld surfaces for the asymmetric unit of ABZ-Cl projected along the stacking direction. An additional ABZ molecule was included on (a) top and (b) bottom to emphasize π-π stacking interactions.

PXRD

PXRD patterns, shown in Figure 4, were obtained from powder samples in order to examine other aspects of ABZ-Cl powder, and differentiate it from I and II solid forms of ABZ. The diffractogram of ABZ-Cl showed a crystalline structure. However, by comparing its pattern with the ones of the ABZ desmotropes[10,] it was confirmed that this salt crystallizes in a different structure. Recrystallized hydrochloride evidenced clear differences in intensity and sharp peaks. The pattern displayed peaks located at 7.2°, 11.8°, 12.7°, 14.2°, 19.1°, 22.5°, 23.5°, 23.8°, 25.8°, 26.9°, 28.8°, 30.3°, 31.7°, 32.8° and 33.9° (2θ), evidencing the formation of other crystal ABZ form. In addition, this powder pattern exhibits a strong correlation with the one calculated by single-crystal X-ray diffraction. Additionally, the influence of environmental temperature on the crystalline form was evaluated by means of a complementary stability testing. Therefore, ABZ-Cl samples were stored in containers protected from light at room temperature. The PXRD patterns, performed after 180 days of storing, showed the characteristic peaks of the crystalline salt, evidencing the physical stability of the sample when it was stored at room temperature. ABZ-Cl conserves its crystalline status.

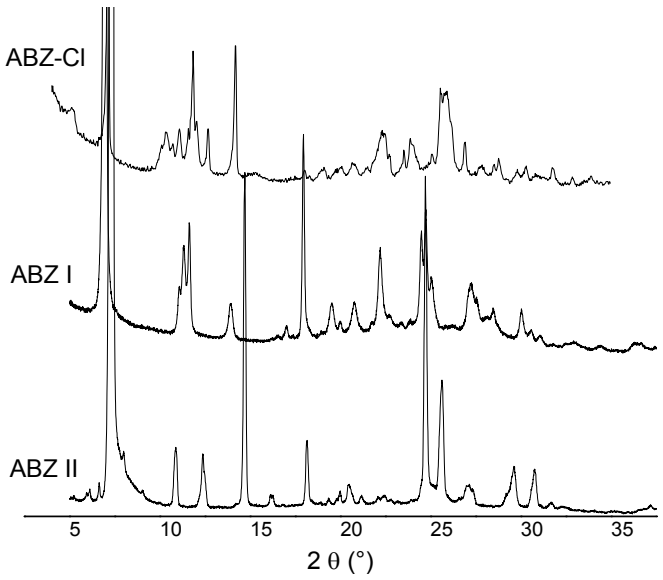

Figure 4. Powder X-ray diffraction patterns of ABZ-Cl, ABZI and ABZII.

1D and 2D ssNMR

Figure 5 displays the ^{13}C CP-MAS spectrum of ABZ-Cl in comparison with the previous reported solid forms ABZ-I and ABZ-II.[10] Assignments were made according to the quaternary and methyl

group carbon edition spectrum (Figure S1 of Supporting Information) and considering the reported solid state ^{13}C NMR spectra of the ABZ desmotropes. HETCOR experiment was also helpful in identifying some ^{13}C peaks (see Figure 6 below). Table S2, in Supporting Information, contains the ^{13}C chemical shifts for the assigned resonances in ABZ-Cl.

As a result of the changes in almost all of the resonances with respect to previously reported solid forms, it was possible to affirm that ABZ-Cl is a new solid form. Consider for example, C14 that appeared at 53.3 and 52.1ppm for ABZ-I and II, respectively, in which case its resonance was at 56.2 ppm in the salt. Other important notable shift occurred in C11, being at 152.1 ppm in ABZ-Cl and at around 160.6 ppm or 162 ppm in forms I and II. Then, considering NMR point of view, ABZ-Cl does not contain traces of the other solid forms (I and II) at least at the noise level. Note that particular splitting observed in resonances of C6 and C9, and a shoulder in C16, are probably due to the presence of two molecules per unit cell, as it was observed from single-crystal X-ray diffraction. In addition, different samples of ABZ-Cl were monitored after six months of storage showing the same ^{13}C spectra, confirming the stability of the sample during that time.

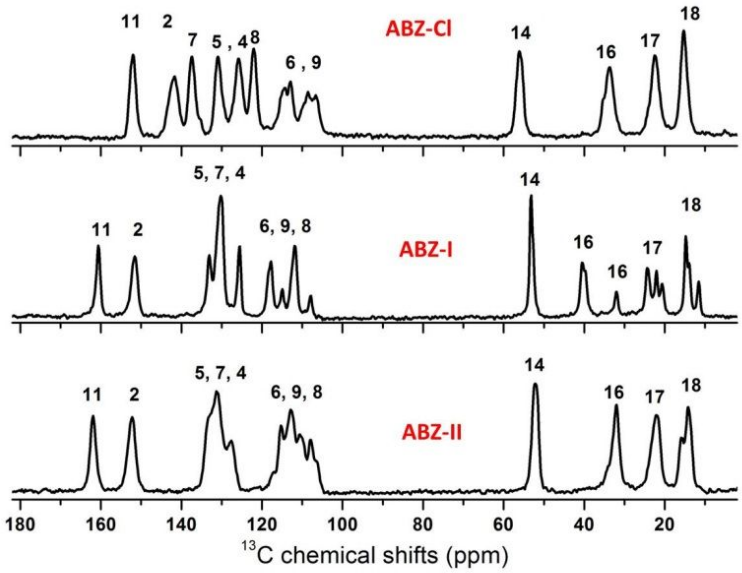

Figure 5. ^{13}C CP-MAS spectra of ABZ-Cl, ABZ-I and ABZ-II. Numbering of peaks in spectra corresponds to that in Scheme1.

Figure 6 shows the 2D ^{1}H-^{13}C HETCOR NMR spectra for ABZ-Cl. A short contact time of 200 μs was used during the CP period allowing only the development of short-range heteronuclear

interactions. The carbon spectrum is shown in the direct projection (horizontal, F2), while the proton spectrum is shown in the indirect dimension (vertical, F1). The clear correlations observed between carbons and their neighbouring protons allowed to extract the proton chemical shifts (see Table S3 in Supporting Information). The 2D spectrum reveals particular inter and intra-molecular correlations, being distinguished from the ones observed for the solid forms I and II of ABZ.[10]

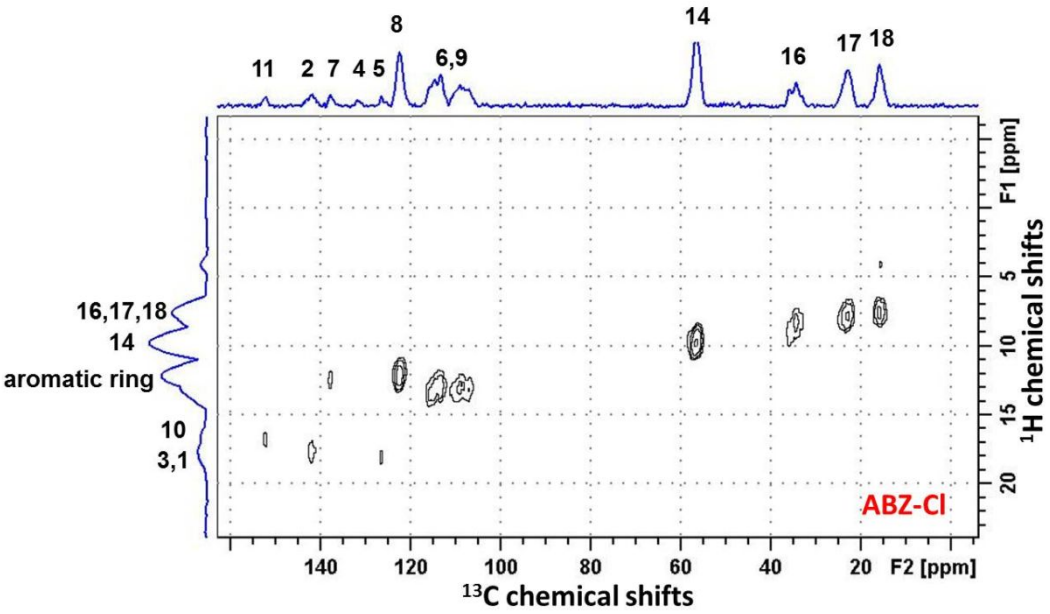

Figure 6. Two-dimensional ^{1}H-^{13}C HETCOR spectrum of ABZ-Cl. ^{13}C and ^{1}H projections are displayed in the direct and indirect frequency dimensions, respectively. Assignments are shown for the carbon and proton spectra.

In particular, there are clear correlations between tail carbons and their corresponding protons. Considering higher ppm signals that belong to NH groups, note the particular correlations, N-H10 with C11, and N1 and N3 with C2. These observations confirm the fact that all nitrogen atoms are protonated, as it was observed from single-crystal X-ray diffraction. In addition, carbons C4, C5 could be assigned from the correlations with H1, H3.

Raman and FT-IR spectroscopy

Raman and FT-IR were performed to analyze the structural changes related to the salt formation, since some characteristic vibrational states may be affected. Therefore, the substantial differences between the spectra of ABZ I and ABZ II desmotropes[10,15] and ABZ-Cl were investigated.

The Raman spectrum of ABZ-Cl exhibited significant spectral differences in the 150–700 cm^{-1} and 1400 and 1800 cm^{-1} regions with respect to the spectra of the solid forms I and II of ABZ [15] (Figure 7). It was possible to identify and unequivocally distinguish this salt from ABZ I and ABZ II.

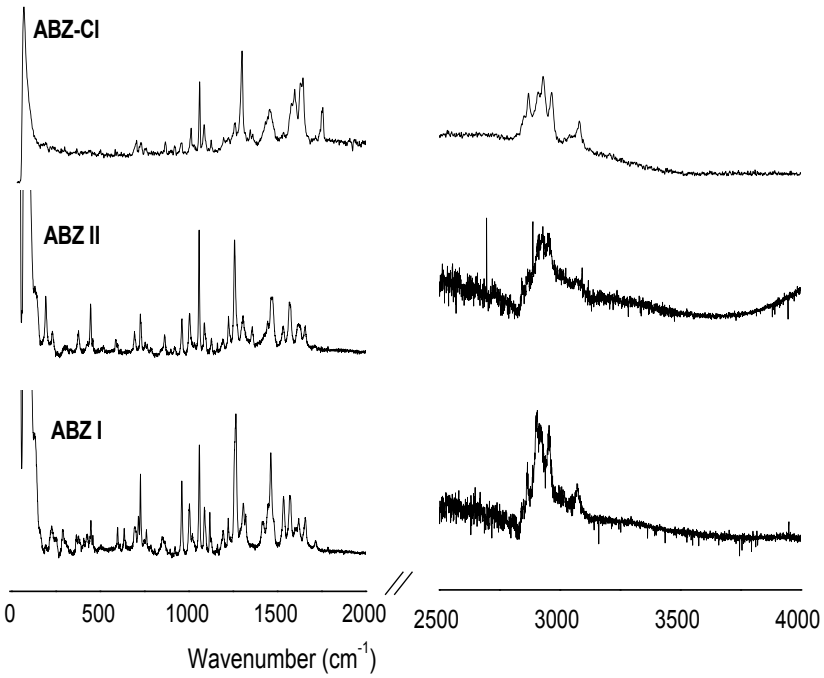

Figure 7. Raman spectra of ABZ-Cl, ABZ I and ABZ II.

The FT-IR spectra (Figure 8) revealed additional evidence to distinguish between the solid forms of ABZ. The assignment of the FT-IR bands for ABZ-Cl are shown in Table S4 (Supporting Information). By comparing the signal spectra, it is possible to observe the N–H stretching vibration intense band localized at 3325 cm^{-1} in the ABZ desmotropes; however, a weak N–H stretching band is observed at lower frequency (3080 cm^{-1}) in the ABZ-Cl spectrum. Additionally, the band corresponding to the carbonyl group of the carbamate moiety appeared shifted to higher frequency (1750 cm^{-1}) with respect to the ABZ desmotropes.[10] The CH_3 absorption appeared as two bands at

1440 and 1489 cm^{-1}, and the C=N stretching bands are localized at 1640 and 1573 cm^{-1}. In addition, the bands in the fingerprint region (between 1500 and 600 cm^{-1}) show marked differences.

In addition, the C=O frequency shift is comparable to the observed for ABZ salt with L-Tartaric acid and salts hydrates with benzene and oxalic acid,[23] which indicate a stronger hydrogen bonding. This spectral modification of ABZ-Cl confirms the intramolecular hydrogen-bond N1H1···O12 observed from single-crystal X-ray diffraction, unlike hydrogen bonds that connect the molecules in the salts reported by Bolla and Nangia.[23]

In this study, the analysis of spectral Raman and FT-IR differences observed for ABZ-Cl with respect to ABZI and ABZII forms and other salts, previously reported, evidenced that the N–H group of the carbamate moiety is involved in the salt formation, suggesting that the hydrogen of the HCl is attached to the N10.

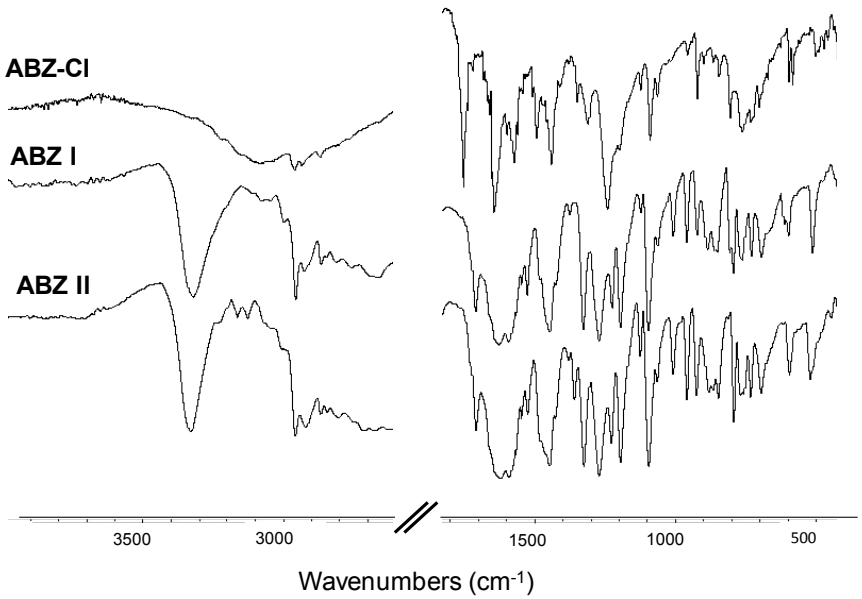

Figure 8. FT-IR spectra of ABZ-Cl, ABZ I and ABZ II.

Thermal analysis

The thermal behavior of solid salt was investigated. The DSC and TGA profiles of ABZ-Cl are shown in Figure 9.

The DSC profile of ABZ-Cl showed the following transitions: an endothermic event at 105°C associated with a mass loss of 3.1% in TGA curve, which can be assigned to the loss of superficial

adsorbed solvent remaining from the synthesis which could be treated of adsorbed water; the next endothermic signal with peak at 173.1 °C (onset at 159.6 °C) and a weight loss of 15.2% in TGA, which is close to the theoretical value expected for the release of HCl (~13%); and the last mass loss of 40.5% beginning at 275°C along with the corresponding endotherm peak at 320.4 °C, which is attributed to the decomposition of ABZ. However, by comparing the thermal curves, a lower thermal stability for the salt ABZ-Cl with respect to ABZ I and ABZ II desmotropes was evidenced.

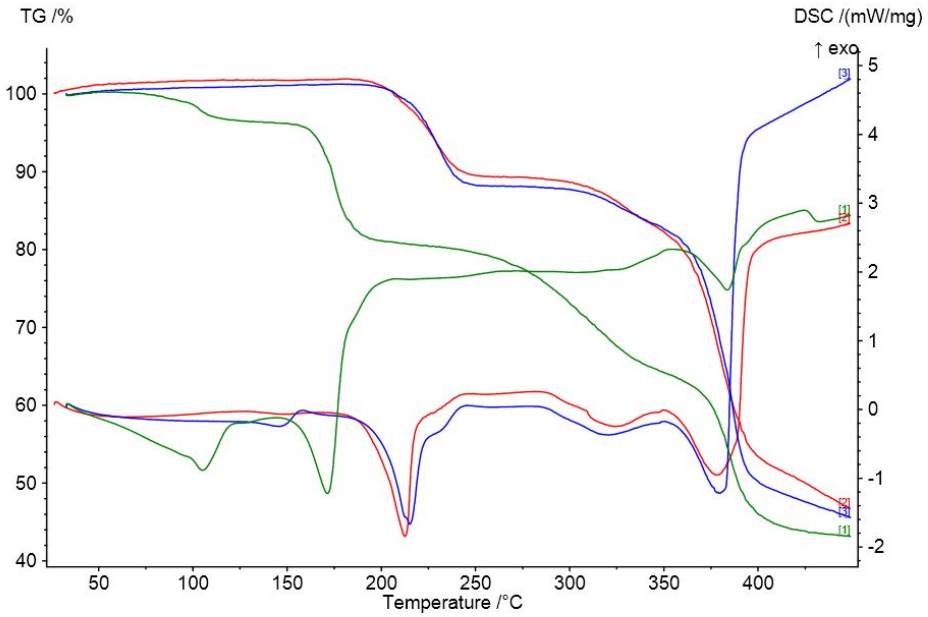

Figure 9. DSC and TGA curves of ABZ-Cl (green), ABZ I (red) and ABZ I (blue).

SEM

The SEM microphotographs (Figure 10) were used to examine the morphological aspect of the salt and, additionally, evaluate differences with respect to forms ABZ I and ABZ II previously reported.[15] The microscopic appearance of the solid offered supporting evidence on the formation of a different solid phase. The images revealed that the size and shape of the particles are very different from each solid. In particular, ABZ-Cl showed a crystalline structure of regular compact particles with rod-like shape and smooth surface, which are adhered adopting a morphology of the starry type. While ABZ I showed irregular particles of different sizes and shapes forming aggregates, ABZ II existed as self-agglomerate lamellar particles.[15]

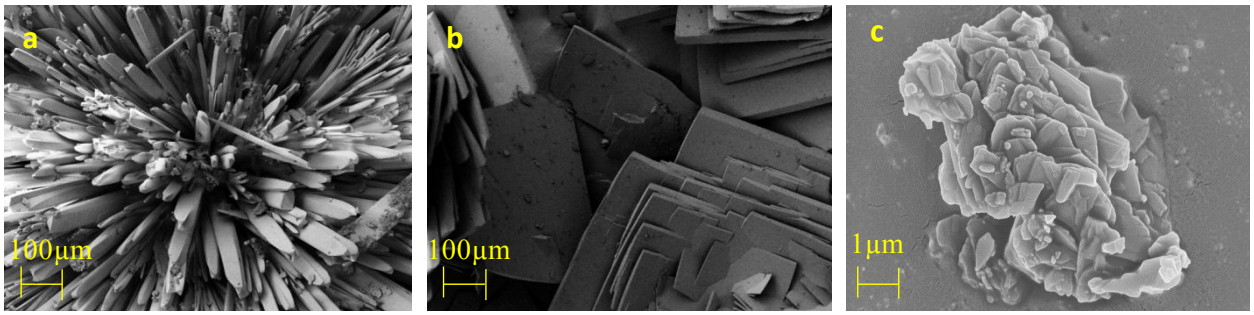

Figure 10. SEM microphotographs of: a) ABZ-Cl, b) ABZ-II and c) ABZ-I.

EDS

EDS, a chemical microanalysis technique,[42] was used in conjunction with SEM to determine the chemical composition of the ABZ-Cl salt. Figure 11 shows the imaging results: spectrum of X-ray energy versus counts and the chemical map for Cl.

EDS analysis evidenced the elemental composition of the sample: C, O, N, S and Cl, confirming that the sample is a hydrochloride salt. In addition, the photomicrograph shows a homogeneous distribution of element Cl in the sample.

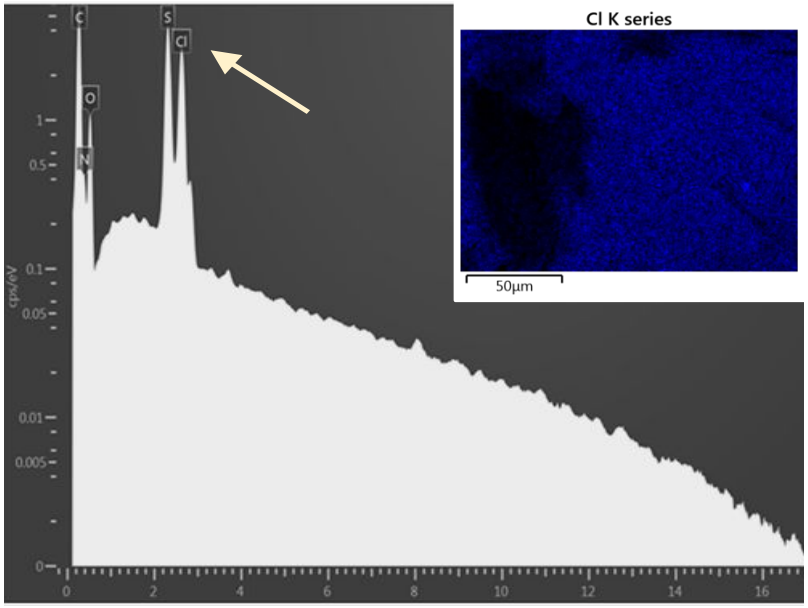

Figure 11. EDS spectrum for ABZ-Cl and chemical map for Cl.

Solubility analysis

The apparent solubility of ABZ-Cl was evaluated at 37.0 ± 0.1 °C. Table 1 summarizes the results obtained in aqueous solution (pH 6.2), SGF (pH 1.2), and SIF (pH 6.8). The solubility data showed that ABZ-Cl is significantly more soluble than the ABZ desmotropes (Figure 12), demonstrating that this salt significantly improves the solubility of the drug at low pH values. In particular, the solubility of ABZ-Cl in aqueous solution showed an increase of 30 times with respect to ABZ I and 15 times for ABZ II.[11]

ABZ is weakly basic in nature, which has pKa values of 2.68 and 11.83. From the solubility values, the effects of the ionization associated with the pH can be observed. The results revealed the highest solubility in SGF due to the presence of the molecule in its ionized-state, while in aqueous solution at final pH 3.8, ABZ-Cl was less soluble, which could be assigned to the presence of a more lipophilic species. On the other hand, a lower solubility of the salt in SIF was determined, with the appearance of a white precipitate during the time necessary to reach the solubility equilibrium. This behavior can be associated with the ionic equilibrium at pH 6.8, with ABZ in low percentage as ionized form. In addition, the potassium ions of buffer could act as counterion of the chloride ion, since potassium is more electropositive than nitrogen, interfering with the amine-chloride association.[43] Therefore, the salt formation is disfavored in alkaline solution, in fact it was confirmed analyzing the solid phases obtained in aqueous and SIF media at the end of the experiment by FT-IR (Figure S2 of Supporting Information)

Interestingly, the feasibility of salt formation constitutes an advantageous strategy to drug solubility enhancement in physiological acid conditions, which could improve the oral bioavailability of ABZ, an BCS class II drug.

Table 1. Summary of ABZ-Cl solubility studies.

Solution	Apparent Solubility (μg/mL)
Water	100 ± 4
SFG	1360 ± 130
SFI	6,2 ± 0,4

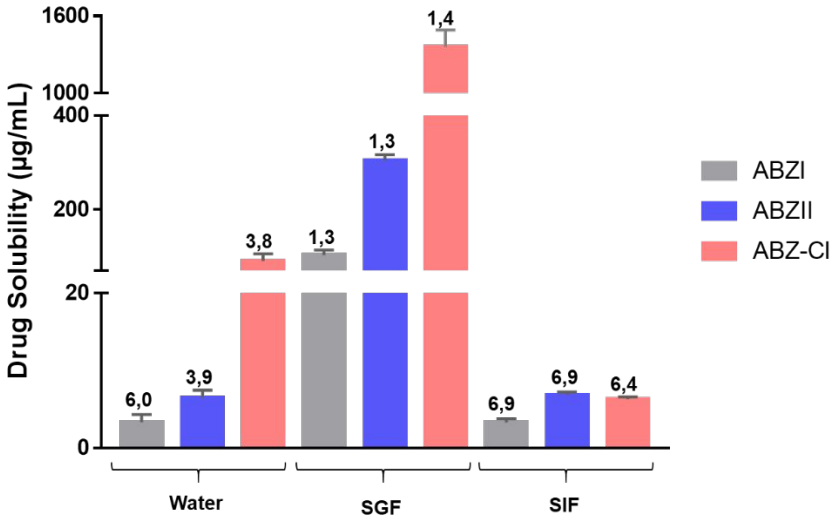

Figure 12. Solubility of ABZ I, ABZ II and ABZ-Cl in water, SGF and SIF, indicating the final pH values of the solution phases.

4. CONCLUSIONS

Important information on a pharmaceutical salt obtained by using a simple and reproducible crystallization method was reported. ABZ-Cl was exhaustively characterized using diverse techniques, providing detailed data on the new solid form. Single-crystal X-ray diffraction data are reported for the first time, highlighting important π- π intermolecular interactions and confirming that all nitrogen atoms are protonated, in agreement with the salt formation. Spectroscopic techniques, together with thermal and microscopic methods, determined significant differences between ABZ-Cl and the desmotropes ABZ I and II previously reported. Raman and FT-IR studies evidenced that the N of the carbamate moiety is involved in salt formation, also confirmed by 2D ssNMR, while EDS/SEM analysis supported the fact that Cl is an element of the solid. In addition, the salt showed physical stability at room temperature. The solubility studies have demonstrated the increasing solubilizing effect of the salt over the pure ABZ. Therefore, ABZ-Cl offers an alternative in the development of new and enhanced formulations of the drug, improving its therapeutic response due to an enhanced solubility.

ACKNOWLEDGMENTS

The authors wish to acknowledge the assistance of Consejo Nacional de Investigaciones Científicas y Técnicas (CONICET) and Universidad Nacional de Córdoba, both providing support and facilities

for this investigation. Besides, project MinCyT-CONICET-CAPES, Secretaría de Ciencia y Técnica de la Universidad Nacional de Córdoba (SECyT-UNC), Fondo para la Investigación Científica y Tecnológica (FONCYT) and the Brazilian agencies CAPES (Finance Code 001), FUNCAP (PRONEX PR2-0101-00006.01.00/15) and CNPq are gratefully acknowledged.

Supporting Information. This report showed the quaternary carbon edition spectrum for ABZ-Cl (Figure S1) and the FT-IR spectra of solid phase at the end of the solubility assays (Figure S2). Moreover, the crystal data and structure refinement for ABZ-Cl (Table S1), the ^{13}C chemical shifts for the assigned resonances (Table S2), the ^{1}H chemical shifts extracted from the correlations in the HETCOR spectrum (Table S3) and the assignment of the FT-IR bands (Table S4) are shown.

REFERENCES

(1) Stephenson LS, Latham MC, Ottesen EA. Malnutrition and parasitic helminth infections. *Parasitology*, **2000**, 121(Suppl):S23–S38.

(2) Kvalsvig JD, Cooppan RM, Connolly KJ. The effects of parasite infections on cognitive processes in children. *Annals of Tropical Medicine and Parasitology*, **1991**, 85:551–568.

(3) Soil-transmitted helminth infections Fact sheet Updated September **2017**. OMS

(4) Ensuring the Efficacy of a Deworming Medicine: Albendazole Chewable Tablets. WHO Drug Information Vol. 29, No. 4, **2015**.

(5) Lacey E. Mode of action of benzimidazoles. *Parasitol. Today,* **1990**, 6:112–115.

(6) García A., Barrera M.G., Piccirilli G., Vasconi M.D., Di Masso R.J., Leonardi D., Hinrichsen L., Lamas M.C. Novel albendazole formulations given during the intestinal phase of Trichinella spiralis infection reduce effectively parasitic muscle burden in mice. *Parasitol. Int.,* **2013**, 62:568–570.

(7) WHO Model Prescribing Information: Drugs Used in Parasitic Diseases – Second Edition. **1995**; 152 pages.

(8) Cook, G. C. Use of benzimidazole chemotherapy in human helminthiases: Indications and efficacy. *Parasitol. Today*, **1990**, 6:133-136.

(9) Horton J. Albendazole: a review of antihelmintic efficacy and safety in humans. *Parasitology*, **2000**, 121

(10) Chattah A.K., Zhang R., Mroue K.H., Pfund L.Y., Longhi M. R., Ramamoorthy A., Garnero C. Investigating Albendazole Desmotropes by Solid-State NMR Spectroscopy. *Molecular Pharmaceutics*, **2015**, *12*:731–741.

(11) Chattah A.K., Pfund L.Y., Zoppi A., Longhi M.R., Garnero C. Toward novel antiparasitic formulations: Complexes of Albendazole desmotropes and β-cyclodextrin. *Carbohydrate Polymers*, **2017**,164:379–385.

(12) Codina A.V., García A., Leonardi D., Vasconi M.D., Di Masso R.J., Lamas M.C., Hinrichsen L.I. Efficacy of albendazole:β-cyclodextrin citrate in the parenteral stage of *Trichinella spiralis* infection. *International Journal of Biological Macromolecules*, **2015**, *International Journal of Biological Macromolecules*, **2015**, 77:203-206.

(13) Ferreira M.J., García A., Leonardi *D.*, Salomon C., Lamas M.C., Nunes T.G.^{13}C and ^{15}N solid-state NMR studies on albendazole and cyclodextrin albendazole complexes. *Carbohydrate Polymers,* **2015**, 123:130-135.

(14) Pradines B., Gallard J.F:, Iorga B.I., Gueutin C., Loiseau P.M., Ponchel G., Bouchemal K. Investigation of the complexation of albendazole with cyclodextrins for the design of new antiparasitic formulations*., Carbohydrate Research,* **2014**, 398:50-55.

(15) Bongioanni A., Sousa Araújo B., Santiago de Oliveira Y., Longhi M.R., Ayala A., Garnero C. Improving Properties of Albendazole Desmotropes by Supramolecular Systems with Maltodextrin and Glutamic Acid., *AAPS PharmSciTech*, 2018, 19:1468-1476.

(16) Pensel P.E., Castro S., Allemandi D., Sánchez Bruni S., Palma S.D., Elissondo M.C. Enhanced chemoprophylactic and clinical efficacy of albendazole formulated as solid dispersions in experimental cystic echinococcosis. *Veterinary Parasitology*, **2014**, 203:80-86.

(17) Jiménez de los Santos C.J., Pérez-Martínez J.I:, Gómez-Pantoja M.E., Moyano J.R. Enhancement of albendazole dissolution properties using solid dispersions with Gelucire 50/13 and PEG 15000. *Journal of Drug Delivery Science and Technology*, **2017**, 42:261-272.

(18) Koradia K., Parikh R.H., Koradia H.D. Albendazole nanocrystals: Optimization, spectroscopic, thermal and anthelmintic studies. *Journal of Drug Delivery Science and Technology*, **2018**, 43:369-378.

(19) Kawabata Y, Wada K, Nakatani M, Yamada S, Onoue S. Formulation design for poorly water-soluble drugs based on biopharmaceutics classification system: Basic approaches and practical applications. *Int J Pharm*, **2011**, 420:1-10.

(20) Stahl P, Wermuth C. Pharmaceutical Salts: Properties, Selection and Use. 2nd Revised Edition. **2011**.

(21) Paulekuhn G. S., Dressman J. B., Saal C. Salt screening and characterization for poorly soluble, weak basic compounds: case study albendazole. *Pharmazie*, **2013**, 68:555-564.

(22) Kourentas A., Vertzoni M., Khadra I., Symillides M., Clark H., Halbert G., Butler J., Reppas C. Evaluation of the Impact of Excipients and an Albendazole Salt on Albendazole Concentrations in Upper Small Intestine Using an *In Vitro* Biorelevant Gastrointestinal Transfer (BioGIT) System. *J Pharm Sci.*, **2016**, 105:2896-2903.

(23) Bolla G.G., Nangia A. Novel pharmaceutical salts of albendazole. *CrystEngComm*, **2018**, 20:6394-6405.

(24) APEX3, Version 2016.1−0; Bruker AXS Inc: Madison, WI, **2012**.

(25) Sheldrick, G. M. SADABS, Version 2008/1; Bruker AXS Inc, **2008**.

(26) SHELXT: Sheldrick, G. M. *Acta Crystallogr., Sect. A: Found. Adv*., **2015**, 71:3−8.

(27) Dolomanov O.V., Bourhis L.J., Gildea R.J., Howard J.A.K., Puschmann H., OLEX2: a complete structure solution, refinement and analysis program, *J. Appl. Crystallogr.*, **2009**, 42:339-341.

(28) Sheldrick G.M. Crystal structure refinement with SHELXL. *Acta Crystallogr. Sect. C-Struct. Chem.*, **2015**, 71:3-8.

(29) Sheldrick G.M. A short history of SHELX, *Acta Crystallogr. Sect. A*, **2008**, 64:112-122.

(30) Battle G.M., Ferrence G.M., Allen F.H. Applications of the Cambridge Structural Database in chemical education, *J. Appl. Crystallogr*., **2010**, 43:1208-1223.

(31) Groom C.R., Allen F.H. The Cambridge Structural Database in Retrospect and Prospect, *Angew. Chem.-Int. Edit*., **2014**, 53:662-671.

(32) Harris, R. K. Nuclear Magnetic Resonance Spectroscopy: A Physicochemical View; Longman Scientific & Technical: Essex, U.K., **1986**.

(33) Metz G., Wu X.L., SmithS.O. Ramped-Amplitude Cross Polarization in Magic-Angle-Spinning NMR. *Journal of Magnetic Resonance, Series A*, **1994**,110:219-227.

(34) Fung, B. M.; Khitrin, A. K.; Ermolaev, K. An improved broadband decoupling sequence for liquid crystals and solids. *J. Magn. Reson.*, **2000**, 142:97−101.

(35) van Rossum, B. J.; Forster, H.; de Groot, H. J. M. High-field and high-speed CP-MAS 13C NMR heteronuclear dipolar-correlation spectroscopy of solids with frequency-switched Lee-Goldburg homonuclear decoupling high-field and high-speed CP-MAS 13C NMR heteronuclear dipolar-correlation spectroscopy of solids with frequency-switched Lee−Goldburg homonuclear decoupling. *J. Magn. Reson*., **1997**, 124:516−519.

(36) Pranzo M.B., Cruickshank D., Coruzzi M., Caira M.R., Bettini R. Enantiotropically related albendazole polymorphs *J. Pharm. Sci.*, **2010**, 99:3731-3742.

(37) Martins F.T., Neves P.P., Ellena J., Camí G.E., Brusau E. V., Narda G.E. Intermolecular contacts influencing the conformational and geometric features of the pharmaceutically preferred mebendazole polymorph C. *J. Pharm. Sci*., **2009**, 98:2336-2344.

(38) Brusau E.V. V, Camí G.E., Narda G.E.E., Cuffini S.L., Ayala A.P., Ellena J. Synthesis and characterization of a new mebendazole salt: Mebendazole hydrochloride. *J. Pharm. Sci*., **2008**, 97:542-552.

(39) Blaton N.M., Peeters O.M., Deranter C.J. (5-Benzoyl-1Hbenzimidazol-2-yl) carbamic acid methyl ester hydrobromide (Mebendazole.HBr), C16H14BrN3O3. *Cryst. Struct. Commun*., **1980**, 9:181-186.

(40) Turner M. J., McKinnon J. J., Wolff S. K., Grimwood D. J., Spackman P. R., Jayatilaka D., Spackman M. A., CrystalExplorer17, **2017**. University of Western Australia. http://hirshfeldsurface.ne.

(41) McKinnon, J. J., Spackman, M. a, & Mitchell, A. S. Novel tools for visualizing and exploring intermolecular interactions in molecular crystals. *Acta crystallographica. Section B, Structural science,* **2004**, 60:627-668.

(42) D' Alfonso A. J., Freitag B., Klenov D., Allen L. J. Atomic resolution chemical mapping using energy-dispersive x-ray spectroscopy. *Physical Review B*, **2010**,81: 100101-R.

(43) Little E. J., Jones M. M. A Complete Table of Electronegativities. *Journal of Chemical Educofion*, **1960**, 37:231-233.

"For Table of Contents Use Only"

Manuscript Title: Investigating a soluble pharmaceutical salt: Albendazole Hydrochloride

Author List:

Agustina Bongioanni

Maria Soledad Bueno

Julieta Abraham Miranda

Ana Karina Chattah

Alejandro Pedro Ayala

Marcela Raquel Longhi

Claudia Garnero

TOC graphic

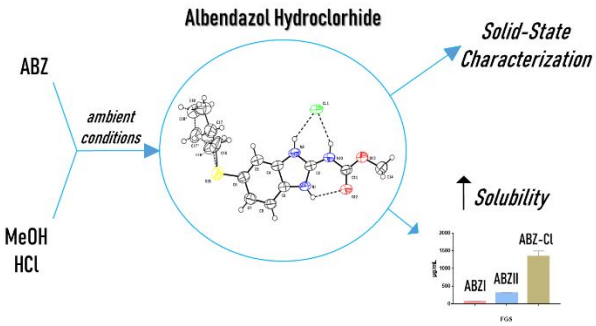

Synopsis

A pharmaceutical salt of albendazole was obtained and characterized by X-ray diffraction, magic angle spinning solid-state nuclear magnetic resonance spectroscopy, Raman and Fourier transform infrared spectroscopies, thermal analysis, energy-dispersive X-ray spectroscopy and scanning electron microscopy. The studies showed the participation of the carbamate moiety in the salt formation. A significant increase in the Albendazole solubility was determined.